

Article

Analyzing Pore Evolution Characteristics in Cementitious Materials Using a Plane Distribution Model

Yezhen Yuan ^{1,2}, Zhe He ³, Kaimin Niu ^{1,3}, Bo Tian ^{1,3}, Liangliang Chen ⁴ , Wei Bai ⁵, Shaopeng Zheng ^{4,*} and Guoman Yu ⁶

¹ School of Civil Engineering, Chongqing Jiaotong University, Chongqing 400074, China; jd.xie@rioh.cn (Y.Y.); km.niu@rioh.cn (K.N.); b.tian@rioh.cn (B.T.)

² Guangxi Nanbai Expressway Co., Ltd., Nanning 530029, China

³ Research Institute of Highway, Ministry of Transport, Beijing 100088, China; z.he@rioh.cn

⁴ Yunnan Provincial Transportation Planning and Design Research Institute Co., Ltd., Kunming 650000, China; chenll@stwip.com

⁵ Guangxi Nantian Expressway Co., Ltd., Nanning 530022, China; hf198507@gmail.com

⁶ Construction Headquarters of Nujiang Beautiful Highway Greenway, Nujiang 673200, China; ynjtgh@126.com

* Correspondence: zhengshaopeng@stwip.com

Abstract: This research aims to analyze the distribution and evolution of pores within the planar structure of cement-based materials. Utilizing digital imaging methods, a model for pore plane distribution was established, and the evolutionary patterns of both total pore numbers and varying pore sizes in cement-based materials were investigated. The research introduced an innovative experimental method for analyzing pore distribution within cement-based planar structures. Additionally, a hybrid method was proposed, combining automated image binarization thresholding with manual comparative analysis, thereby enhancing the feasibility of comparative research. Pores were categorized into four distinct sizes: tiny pores (5–200 μm), small pores (200–500 μm), medium pores (500–1000 μm), and large pores (>1000 μm). Areas with apertures <5 μm were classified as dense areas. The findings indicated that the overall number of pores in cement-based materials increased due to the influence of styrene butadiene latex additives. However, at a 15% dosage, the rate of pore formation reached an inflection point, confirming that various factors, such as styrene butadiene latex, air bubbles, and the cement-based material itself, collectively influenced pore formation. The research also demonstrated that styrene butadiene latex affected the four categorized pore sizes differently. Importantly, a higher latex dosage did not necessarily lead to a proportional increase in pore content. Pore content was influenced by multiple factors and exhibited different distribution patterns. The number of micropores, although relatively small, gradually increased with higher latex dosages, while small and medium pores generally showed an upward trend. At a 10% latex dosage, both small and medium pores reached a turning point in their rate of increase. Large pores also exhibited a general increase, peaking at a latex dosage of 10%. It was confirmed that both the total pore volume and the content of micropores were critical factors in determining the mechanical properties of cementitious materials. Higher porosity and micropore content generally weakened mechanical performance. However, at a small latex dosage, there was an improvement in flexural strength. When the latex dosage reached 15%, the total pore and micropore content declined, resulting in a balanced increase in flexural strength and a mitigated decline in compressive strength. This study offers valuable insights into the evolution of total pore volume and the content of pores of various sizes, providing a theoretical basis for the meticulous selection of additive types and dosages from a microscopic perspective.



Citation: Yuan, Y.; He, Z.; Niu, K.; Tian, B.; Chen, L.; Bai, W.; Zheng, S.; Yu, G. Analyzing Pore Evolution Characteristics in Cementitious Materials Using a Plane Distribution Model. *Coatings* **2023**, *13*, 2023. <https://doi.org/10.3390/coatings13122023>

Academic Editor: Bohayra Mortazavi

Received: 26 October 2023

Revised: 27 November 2023

Accepted: 28 November 2023

Published: 29 November 2023



Copyright: © 2023 by the authors. Licensee MDPI, Basel, Switzerland. This article is an open access article distributed under the terms and conditions of the Creative Commons Attribution (CC BY) license (<https://creativecommons.org/licenses/by/4.0/>).

Keywords: cementitious materials; stomatal plane distribution model; digital images; pore evolution characteristics

1. Introduction

Cementitious materials are of paramount importance in road engineering due to their multiphase porous systems. Understanding the distribution patterns of pore structures is crucial for ensuring both durability and sustainable performance. Factors such as pore number, size, and distribution patterns within these materials directly influence the mechanical properties and durability [1]. The internal pore structure of cementitious materials indeed plays a fundamental role in defining their overall performance. To enhance specific aspects of cementitious materials, additives are commonly employed. For example, butylbenzene latex polymers are added to cement concrete to improve its impermeability [2,3]. Styrene butadiene latex, a block copolymer, has been the subject of extensive research regarding its impact on the microscopic pore structure of cementitious materials. Li et al. discovered that the incorporation of styrene butadiene emulsion shifted the pore size distribution in cementitious materials toward micropores, which also had an effect on their macroscopic mechanical properties [4]. Zhang et al. demonstrated that polymer emulsions influence the pore structure of cement mortar, resulting in an increased proportion of smaller pores [5]. Yang emphasized that a decrease in the proportion of smaller pores has a negative impact on the mechanical properties and frost resistance of cement concrete [6]. Sakai et al. conducted a study on the effects of water-reducing agents on the pore structure of hardened cement, outlining the variations in different pore sizes [7]. Kondraivendhan et al. established a relationship between the compressive strength of cement slurry and the average pore distribution radius, affirming the practical value of such a relationship [8].

Zhang et al. conducted a study on the impact of polymer emulsion on concrete's pore structure. They observed that an increased admixture of polymer emulsion led to a reduction in smaller pores (within 100 μm) and an increase in larger pores (above 400 μm), thereby having a detrimental effect on the material's mechanical properties [9]. Wu et al. categorized pores in cementitious materials into four size-based classes, including benign pores (below 200 nm). Their argument highlighted that an increase in the number of pores smaller than 50 nm and a decrease in those larger than 100 nm contribute to the material's durability [10,11]. Jinteng et al. differentiated pores in cementitious materials into gel microcrystalline endospores (1.2 nm), gel pores (0.6–1.6 nm), capillary pores (3.2–200 nm), and macropores (above 200 nm). They emphasized that pores larger than 10 nm have a significant impact on frost resistance [12]. Jawed et al. also investigated pore structures, classifying them into macropores (above 5 μm) and capillary pores. Capillary pores were further subdivided into large capillary pores (50–5000 nm), interstitial pores (2.6–50 nm), and micropores (2.6 nm) [13]. This classification closely aligns with that of Jinteng et al. [12]. Macropores were identified as the primary contributors to the mechanical and durability properties of cementitious materials. The European Concrete Board's CEB Guide for the design of durable concrete structures specified that pore sizes between 0.1 and 10 nm are considered micropores, 10–10,000 nm are capillary pores, and pores larger than 10,000 nm are macropores. Pores exceeding 1000 μm in size were explicitly mentioned as introducing air holes, which significantly deteriorate the performance of cementitious materials [14,15]. F.H. introduced a pore classification system that included micro, delicate, and macro scales while studying cementitious materials [16]. IO.C. et al. classified cementitious materials by pore size into gel pores (below 1000 nm) and highlighted that pores larger than 10 μm were considered macropores [17]. Yan and Yang et al. referred to pores in cementitious materials larger than 10 μm as stomata. Their observations indicated that general air-entraining agents introduce more stomata ranging from 10 μm to 200 μm , followed by 200 μm to 500 μm stomata, with the fewest stomata being larger than 500 μm [18,19].

Several studies have provided valuable insights into the internal pore structure of cementitious materials and the influence of external factors [20–25]. Most of these studies have focused on the distribution of air bubbles in freshly mixed cementitious materials and the rules governing pore changes within the three-dimensional internal structure. The primary tools used for these analyses are often costly instruments such as mercury

pressure instruments, and the scale of study is mainly in the nanometer range or smaller. However, there has been limited research on the evolution of pore structures within the two-dimensional cross-section of cementitious materials after hardening and the impact of these two-dimensional pore distribution characteristics on the mechanical properties of cementitious materials.

Building upon the existing research, this study aims to address specific test constraints, such as the minimum particle size of the white powder used to fill pores, which is 5 μm . Recognizing that smaller pore structures have a less adverse impact on the performance of cementitious materials and contribute to greater internal compactness, a 5 μm threshold is established as the boundary between compact and porous areas. Specifically, the study focuses on pores larger than 5 μm ; regions with pore sizes smaller than 5 μm are designated as compact areas. Furthermore, given the substantial influence of pores larger than 1000 μm on the properties of cement mortar, these are classified as areas of large porosity. For pore sizes ranging between 5 and 1000 μm , pores are further categorized into tiny (5–200 μm), small (200–500 μm), and medium (500–1000 μm) groups. The planar distribution model, as depicted in Figure 1, serves as the foundational tool for the analysis of pore distribution in cementitious materials. This model characterizes various pore distribution ratios based on two-dimensional planar area sizes and classifies them according to pore aperture size. This framework offers an intuitive comprehension of the proportion and attributes of different pore sizes within the cementitious material. By adjusting the ratio within each category, the model can depict the overall pore distribution and the specific sizes of individual pores, providing a theoretical framework for future investigations into the evolution of internal pore distribution in cementitious materials.

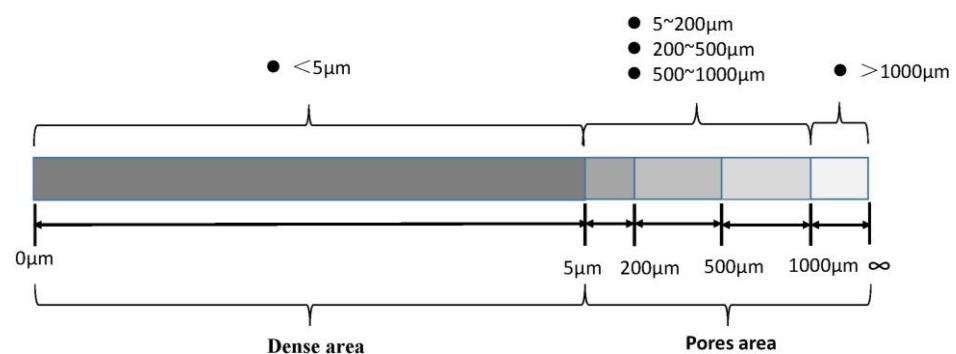


Figure 1. Pore plane distribution model. (<5 μm , 5–200 μm , 200–500 μm , 500–1000 μm , >1000 μm).

To address this gap, the study establishes a planar distribution model for the pore structure in cementitious materials. A low-cost, easy-to-operate digital imaging method is introduced to analyze the pore structure evolution in hardened cementitious materials. By utilizing styrene butadiene latex polymer as the external influencing factor and focusing on the micron-sized pore scale, the development and evolution patterns of cementitious materials' pore structures are examined in the study. The objective is to gain insights into the effects of two-dimensional planar microscopic pore distribution on the mechanical properties of cementitious materials. This study provides a theoretical foundation for enhancing the properties of cementitious materials and offers a simple and accurate experimental evaluation method to ensure their sustainable development.

2. Materials and Methods

2.1. Raw Materials

To investigate the characteristics of pores in cementitious materials, styrene butadiene latex polymer is used as a modifying factor for the internal pore structure. The concentration of the polymer is adjusted to analyze alterations in the internal pore structure of the cementitious materials. These adjustments are expressed as a percentage of the total cement mass and are detailed in Table 1.

Table 1. Mix proportions for test.

Serial Number	Water (g)	Cement (g)	Standard Sand (g)	Latex (g)	Defoamer (g)	Latex Dosage (%)
1	225	450	1350	0	0	0
2	213.53	450	1350	22.5	4.12	5
3	202.05	450	1350	45.0	4.18	10
4	190.58	450	1350	67.5	4.25	15
5	179.10	450	1350	90.0	4.31	20

For the experimental setup, ordinary Portland cement (P.O 42.5) and sand were used in accordance with ISO standard specifications. Test water meeting all relevant criteria was used. Throughout the experiment, a consistent water–cement ratio of 0.5 was maintained, with unaltered cement and standard sand dosages. To mitigate the adverse effects of harmful pores produced by styrene butadiene latex in cementitious materials [26–28], a defoamer was added to the mixture. The defoamer constituted 6% of the total mass of water, cement, and latex, aligning with real-world engineering standards. Experimental mix proportions for the test are detailed in Table 1, while the key properties of the selected styrene butadiene latex polymer are presented in Table 2.

Table 2. Basic performance of styrene butadiene latex.

Solid Content (%)	PH	Viscosity (20 °C) (mPa.s)	Char Yield (450 °C) (%)	Glass Transition Temperature (°C)
47.0	8.25	48.02	15.4	10.2

2.2. Methods

Cement mortar specimens were molded into dimensions of 150 mm × 150 mm × 60 mm. After curing for 28 days, they were cut and smoothed into planar samples measuring 150 mm × 150 mm × 30 mm for testing. From these samples, a 100 mm × 100 mm section was selected and coated with a non-fading black oil-based pen as a primer. This coating was allowed to dry at room temperature for a minimum of two hours. Subsequently, white powder with a particle size of 5 µm was applied to fill the surface pores of the sample [29]. Excess powder was removed, ensuring that only the pores were filled while leaving the black-coated background exposed. The specimen preparation primarily involved three stages: molding, cutting and smoothing, and pre-treatment. These processes are illustrated in Figure 2.

An EOS 2000D camera, Canon (Tokyo, Japan), equipped with a CMOS sensor boasting an effective pixel count of 24.1 million and an optical viewfinder, was employed for capturing images of specimen cross-sections under even, shadowless illumination. MATLAB software (Version Number: R2023) was utilized for grayscale conversion and binarization. This method allowed for the analysis of pore distribution on the specimen’s surface using digital imaging techniques. Based on the pixel values in the captured images [30–32], “1” was used to represent white powder-filled pores after binarization, while “0” denoted unfilled areas in black, signifying denser regions (as depicted in Figure 3a). Although grayscale binarization is a widely adopted technique, the selection of the threshold is of utmost importance. Various options are typically considered, including using 0.5 as a starting point, computing the average grayscale values, or employing an automated method to determine the threshold. It is worth noting that each of these methods comes with a certain margin of error.

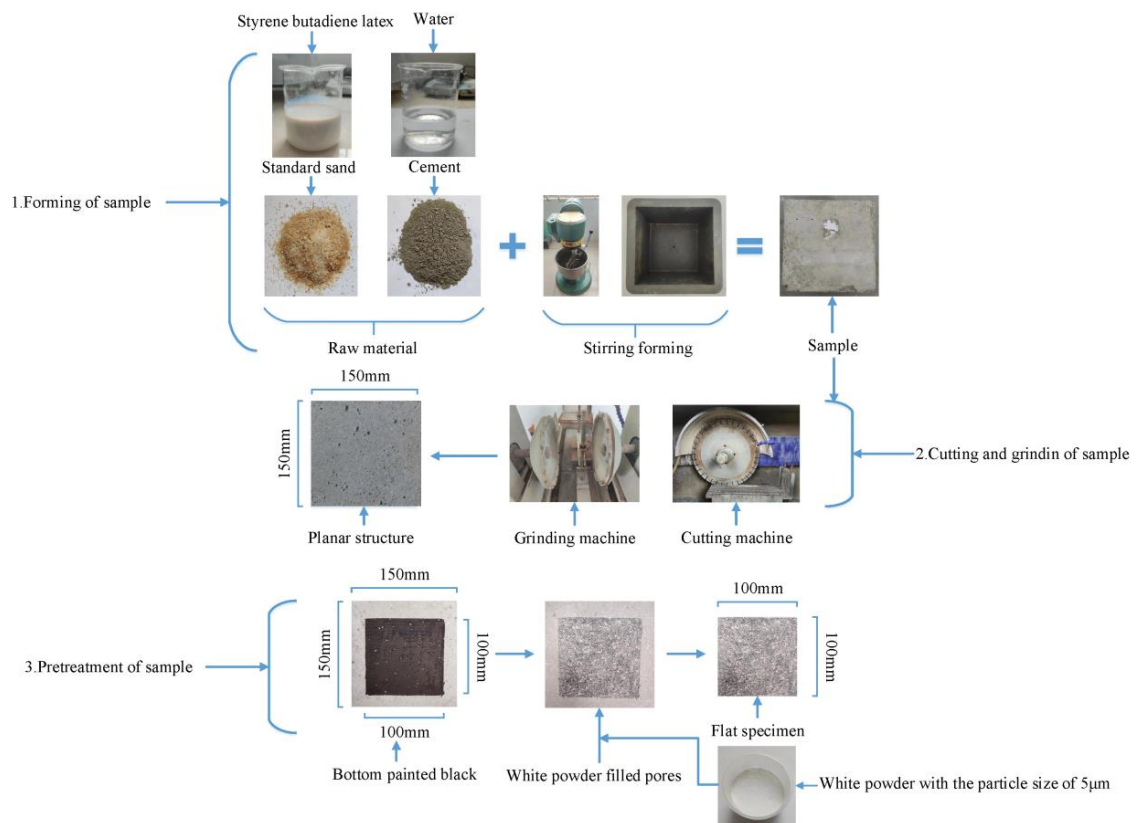


Figure 2. Flow chart of sample preparation process.

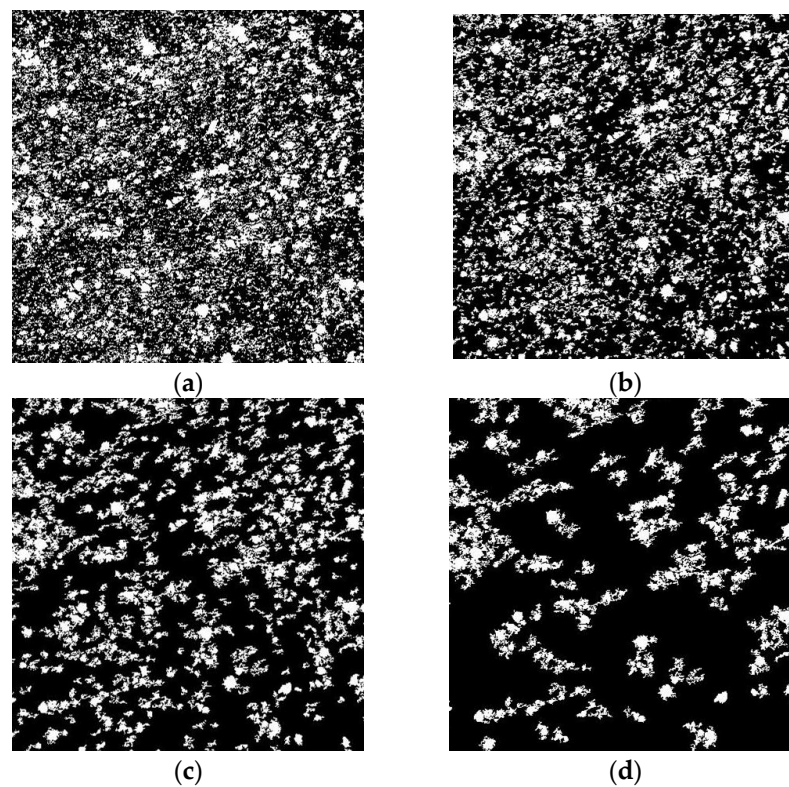


Figure 3. Schematic diagram of sample digital image processing. (a) Schematic diagram of sample binarization treatment; (b) Schematic diagram of aperture > 200 µm pores; (c) Schematic diagram of aperture > 500 µm pores; (d) Schematic diagram of aperture > 1000 µm pores.

In this study, MATLAB was initially employed to automatically determine the binarization threshold, which was set at 0.6. Subsequently, manual adjustments were made by incrementally increasing or decreasing the threshold by 0.05 and 0.1, ultimately arriving at the optimal threshold of 0.65. By combining automated threshold confirmation with manual fine-tuning, the binarization threshold was refined to closely align with the actual image characteristics, thereby establishing a dependable foundation for the experimental investigation. While this approach could be influenced by subjective factors, its feasibility and accuracy are generally sufficient for conducting comparative studies under consistent conditions.

Within the experimental framework, the pixel value range was considered in relation to the actual dimensions of the 100 mm × 100 mm planar section. The values “1” and “0” in the binarized image were designated as Z_1 and Z_0 , respectively. The sum of Z_1 and Z_0 constituted the total pixel value, represented as Z . The total porosity content, denoted as P_1 , was equivalent to Z_1 . Therefore, the total content, P_1 , is calculated as follows:

$$P_1 = Z_1 / Z \quad (1)$$

The actual cross-sectional area is denoted as $S = 0.01 \text{ m}^2$, and the number of pixel points Q per unit area is represented as follows:

$$Q = Z / S \quad (2)$$

In the study, the maximum particle size of the white powder used for pore filling was 5 μm . As a result, pores smaller than this threshold remained unfilled, manifesting as black regions in the digital images. Taking advantage of this scale effect, pixel values corresponding to pores filled with white powder were extracted. Assuming the pores to be approximately circular, the formula πr^2 was utilized to calculate the number of pixel points representing pore sizes of 200 μm , 500 μm , and 1000 μm , denoted as Z_{200} , Z_{500} , and Z_{1000} , respectively.

$$Z_{200} = (\pi r_{200}^2) * Q$$

$$Z_{500} = (\pi r_{500}^2) * Q$$

$$Z_{1000} = (\pi r_{1000}^2) * Q$$

During the digital image processing, the MATLAB function `bwareaopen` was utilized to remove objects with areas smaller than Z_{200} , Z_{500} , and Z_{1000} from the binary images. Consequently, the number of pixel points exceeding 200 μm , 500 μm , and 1000 μm , denoted as $Z_{>200}$, $Z_{>500}$, and $Z_{>1000}$, were obtained, as depicted in Figure 3b–d. The corresponding contents of stomata larger than 200 μm , 500 μm , and 1000 μm , labeled as P_{200} , P_{500} , and P_{1000} , were calculated as follows:

$$P_{200} = Z_{>200} / Z$$

$$P_{500} = Z_{>500} / Z$$

$$P_{1000} = Z_{>1000} / Z$$

The stomatal contents for <200 μm , 200–500 μm , 500–1000 μm , and >1000 μm were calculated as follows for $P_{<200}$, $P_{200-500}$, $P_{500-1000}$, and $P_{>1000}$.

$$P_{<200} = P_1 - P_{200}$$

$$P_{200-500} = P_{200} - P_{500}$$

$$P_{500-1000} = P_{500} - P_{1000}$$

$$P_{>1000} = P_{1000} = Z_{>1000} / Z$$

The methods outlined above yielded insight into the spatial distribution of internal pores in cementitious materials during the continuous hardening process. Evolving trends in pore content across different size ranges were observed, and a planar porosity model supported by extensive experimental data was constructed. This model served as a theoretical foundation for the analysis of the mechanical properties and durability of cementitious materials.

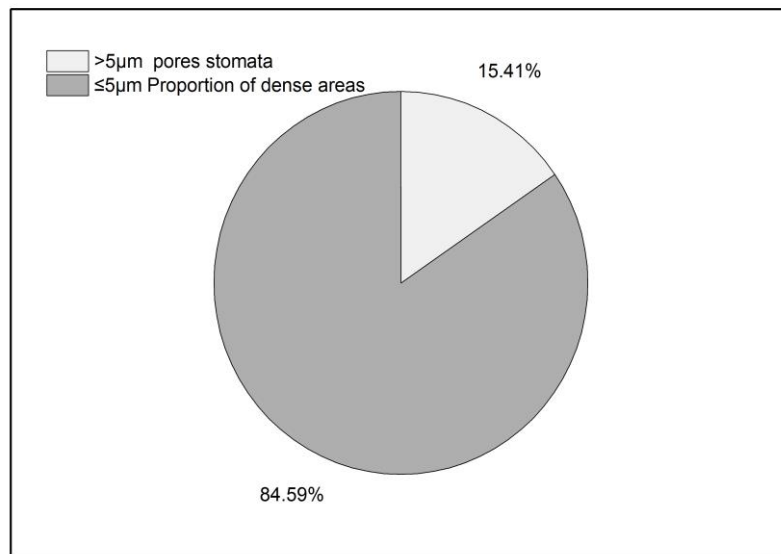
The methods outlined above yielded insights into the spatial distribution of internal pores in cementitious materials during the ongoing hardening process. Evolving trends in pore content across different size ranges were observed, and a planar porosity model, supported by extensive experimental data, was constructed. This model serves as a theoretical foundation for the analysis of the mechanical properties and durability of cementitious materials.

3. Results and Discussion

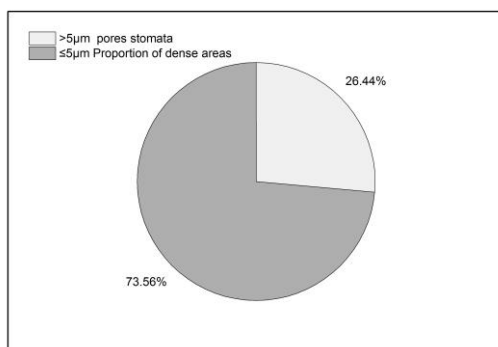
3.1. Analysis of Evolutionary Pattern of Total Stomatal Volume

In cementitious materials, the blending of various components gave rise to a complex solid–liquid–gas three-phase system, leading to the formation of a porous structure within the cement mortar. The porosity was governed by the intrinsic properties of the material [33–35]. Styrene butadiene latex, as an additive in cementitious materials, also constituted a solid–liquid–gas three-phase mixing system, which inevitably influenced the formation and evolution of internal pores to a certain extent. The study focused on hardened cement mortar, in which internal air bubbles underwent a multi-stage formation process. The first stage was the initiation phase, during which air bubbles were introduced into the fresh mortar mix within the complex solid–liquid–gas three-phase system. The second stage was characterized by disorder, as bubbles rearranged, compressed, merged, and escaped due to external forces such as stirring and compaction applied to the fresh mortar. This was followed by a sub-stabilization stage, where the bubbles gradually transitioned from a disordered state to a more stable one under standard temperature and humidity conditions. However, they were still influenced by factors such as cement hydration and water evaporation during the mortar’s hardening process. Finally, in the stabilization stage, which typically occurred after 28 days of curing, the internal pores attained a fixed structural pattern. Specimens for this study were sourced from this last stage.

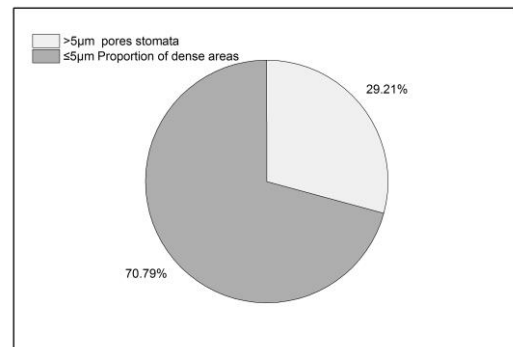
Figure 4 illustrates the impact of butylbenzene latex on the total number of internal pores in cementitious materials. In comparison to latex-modified mortar, the standard mortar exhibited the fewest pores, highlighting that latex inclusion increased the overall pore content within the hardened mortar plane. As the concentration of styrene butadiene latex increased, there was a general upward trend in the total pore count within the mortar. Interestingly, at a 15% latex dosage, the data revealed a turning point: the total pore count decreased to levels comparable to those observed at a 5% dosage. However, with further increases in latex concentration to 20%, the pore count within the hardened mortar plane continued to rise, albeit at a slower rate of increase—only 5.31% compared to the 10% latex dosage.



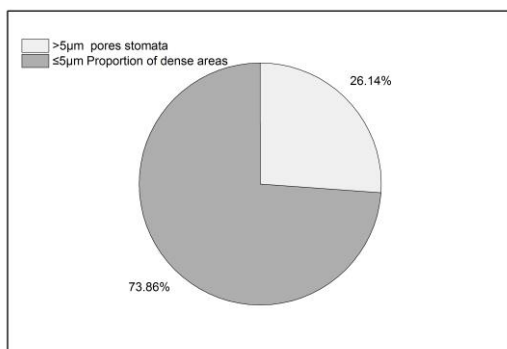
(a) Standard mortar (mix ratio 1)



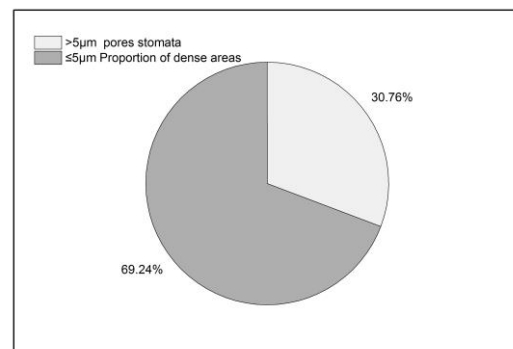
(b) Latex dosage of 5% (mix ratio 2)



(c) Latex dosage of 10% (mix ratio 3)



(d) Latex dosage of 15% (mix ratio 4)



(e) Latex dosage of 20% (mix ratio 5)

Figure 4. Evolution law of total porosity in cement-based materials.

Styrene butadiene latex is a material characterized by a three-phase system of solid–liquid–gas. When utilized as an additive in mortar, its adhesive properties enhance the interface between the mortar and air. This facilitates the introduction of air into the interior of the mortar. The adhesive qualities of the latex compound this effect, making it more challenging for internal pores to escape. As a result, the hardened mortar experienced an increase in the total number of planar pores.

At a low latex dosage of 5%, the latex dispersed non-uniformly within the cementitious material. The bubbles also exhibited uneven dispersion, occupying various spatial positions. The mutual compression and merging of these bubbles were relatively limited at this stage. Consequently, the environment favored the formation of bubbles, leading to a doubling of porosity under this lower latex dosage. As the latex dosage increased, the dispersion gradually transitioned from isolated to more uniform within the cementitious material. Simultaneously, the number of bubbles increased, and they began to occupy shared spatial locations more frequently. This heightened the mutual compression, merging, and rupture of bubbles, creating fluctuations in porosity levels.

Upon reaching a latex dosage of 15%, the total number of pores in the mortar began to decrease. This decline was attributed to increased competition for limited spatial positions, leading to some bubbles being compressed and escaping, ultimately reducing the overall pore count in the hardened mortar. With a further increase in latex dosage to 20%, the number of introduced bubbles also increased. However, these additional bubbles began to rupture and reduce each other's numbers. As some bubbles escaped and formed transient channels, the total porosity of the mortar experienced a slight increase. This suggests that, due to interactions among the bubbles, the pore count cannot increase indefinitely, even with higher latex concentrations.

3.2. Analysis of Stomatal Evolution Patterns of Different Pore Sizes

In cementitious materials, pores of varying sizes are distributed throughout. According to the planar distribution model, these pores fell into four main categories: micropores (5–200 μm), tiny pores (200–500 μm), medium pores (500–1000 μm), and large pores (>1000 μm). The addition of styrene butadiene latex polymer as an additive introduced a considerable number of air bubbles into the cement mortar. This not only influenced the total number of pores after the material had hardened but also affected the sizes of these pores to varying degrees. From the perspective of performance enhancement, the goal was to maintain or increase the total number of pores, particularly favoring smaller pores. Smaller pores were more favorable for improving various performance indicators, such as mechanical strength and durability. However, the specific distribution of different pore sizes within cementitious materials, influenced by the addition of latex, and how this pore structure evolved from the fresh mix to the hardened state, needed to be verified through experimental tests.

Using standard cement mortar (test mix ratio 1) as a reference, Figure 5 reflects the planar distribution of pores of various sizes within the standard mortar. Pores smaller than 5 μm were categorized as the dense region, constituting 84.59% of the plane cross-section of the standard mortar. The remaining 15.41% was occupied by pores of different sizes: 5–200 μm pores accounted for 2.46%, 200–500 μm pores represented 4.61%, 500–1000 μm pores made up 5.36%, and pores larger than 1000 μm constituted 2.98%. The distribution exhibited a characteristic pattern: fewer pores at the extremes and more in the middle ranges. Using this standard mortar as a benchmark, the analysis of pore distribution across different size ranges in cementitious materials impacted by external factors formed the basis for understanding changes in material performance at the microstructural level.

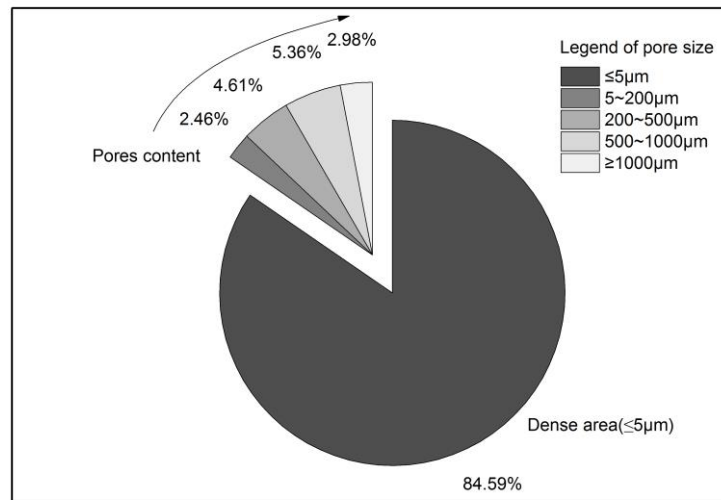
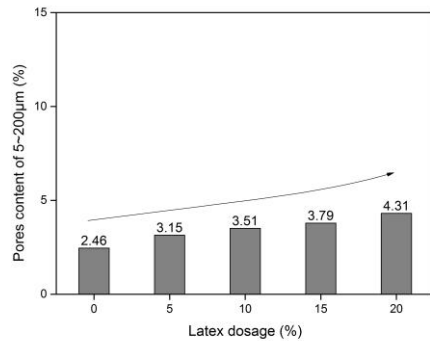
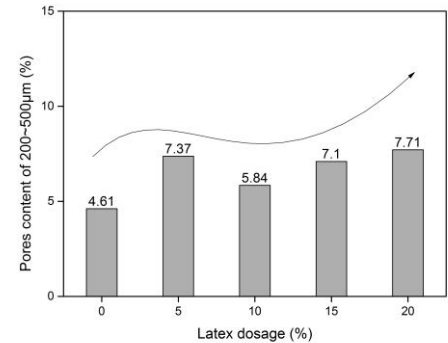


Figure 5. Plane distribution of pores with different pore sizes in standard mortar.

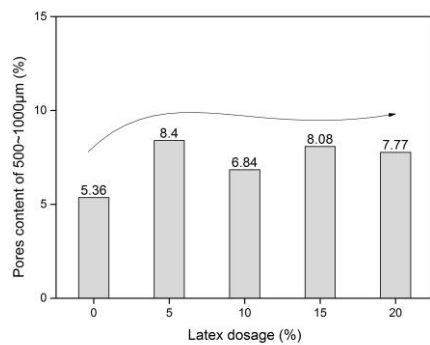
An experimental investigation was undertaken to analyze the distribution characteristics of pores of different sizes in cementitious materials. In this study, the control group consisted of standard mortar without latex, while the primary focus was on latex-modified mortar with varying levels of latex. Figure 6 illustrates the evolution of pore content across different size ranges. Significantly, the control group (standard mortar) exhibited the lowest pore content in all size categories, affirming that the addition of styrene butadiene rubber latex generally increased pore content within each category.



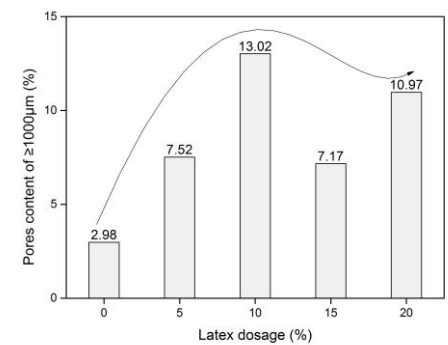
(a) Pore content of 5~200 μm



(b) Pore content of 200~500 μm



(c) Pore content of 500~1000 μm



(d) Pore content of ≥ 1000 μm

Figure 6. Evolution law of pores with different sizes.

Within the 5–200 μm pore size range, the content of pores in latex-modified mortar progressively increased with higher levels of latex doping. The most substantial increase was observed in the data corresponding to a 20% latex doping. In comparison to the standard mortar, the pore content in this range increased by 75.2%. This suggests that the introduction of latex as an admixture led to a shift in the distribution of tiny pores (5–200 μm) in cementitious materials, resulting in increased pore content.

In the pore size ranges of 200–500 μm and 500–1000 μm , a similar pattern of evolution in pore content was observed. With a low latex dosage of 5%, both types of pores exhibited exponential growth. When the latex dosage reached 10%, there was a noticeable change in the growth of pore content. In comparison to the standard mortar, the pore content increased by 26.68% and 27.61% in these size ranges, respectively. As the latex dosage continued to increase, the pore content exhibited a wave-like growth trend. This analysis revealed that at lower latex dosages, the latex was relatively isolated and unevenly distributed within the cementitious material. In this state, there was ample space for the bubbles, weak interactions between them, and limited introduction of bubbles into the mortar, which were conducive to the formation of porosity.

As the latex levels increased, its distribution within the cementitious material became more uniform, as depicted in Figure 7. This led to increased competition for space among the bubbles, more frequent interactions, and intensified processes of bubble extrusion, merging, and rupture. Some bubbles grew into larger sizes, some were crushed due to extrusion, and others escaped the confines of the cementitious material. These intricate internal changes resulted in an oscillatory trend in pore content. However, higher latex dosages altered the solid–liquid–gas three-phase system within the cementitious material, leading to a general increase in the content of both types of pores.

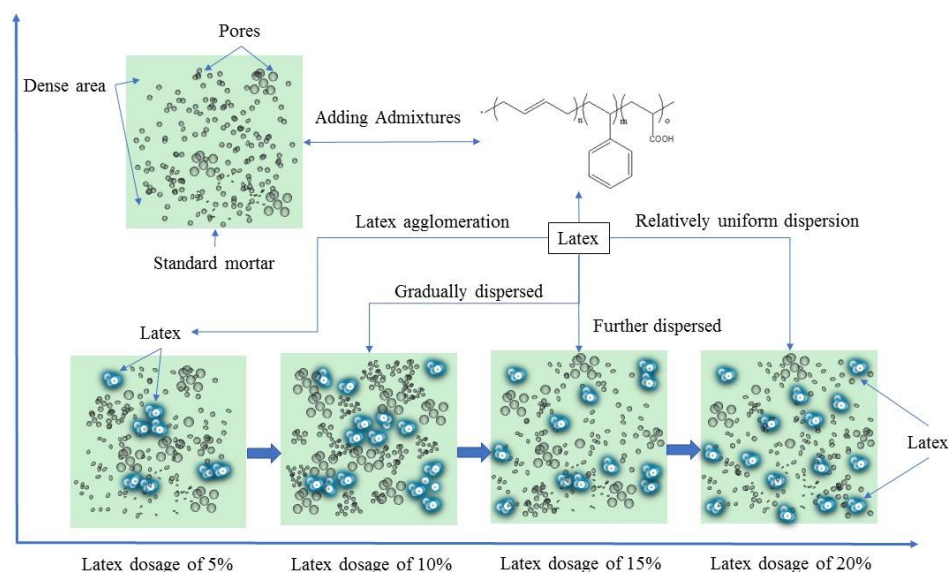


Figure 7. Schematic diagram of dispersion pattern of latex in cement-based materials.

Pore sizes exceeding 1000 μm are categorized as macroporosity, which is known to have detrimental effects on the mechanical properties and durability of cementitious materials, as referenced in [10–21]. Hence, we sought to minimize the presence of these large pores. The test data presented in Figure 6 indicates that standard mortar had the lowest macropore content (>1000 μm) compared to the other pore size ranges, such as 200–500 μm and 500–1000 μm . This low macropore content contributed to the superior performance of the standard mortar.

As the quantity of the latex additive increased, the macropore content in the latex-modified mortar displayed a significant overall upward trend. With a low dosage of 5%, the macropore content essentially doubled. The most substantial increase was observed

at a 10% latex dosage, where the macropore content in the latex-modified mortar was 4.37 times that of the standard mortar. When the dosage reached 20%, the macropore content was 3.68 times that of the standard mortar. With increasing latex dosages, the dispersion state of the latex within the cementitious material underwent significant changes. Initially, it was isolated and unevenly distributed, but it eventually became uniformly dispersed within the cementitious matrix. During this transition, the spatial conditions for the bubbles introduced by the latex also changed significantly, shifting from relatively spacious to increasingly crowded. This led to heightened bubble interactions, including rupture, merging, and escape, which in turn drastically increased the content of large pores. This escalation had a particularly adverse impact on the mechanical properties of the cementitious materials.

Figure 8 presents the total pore count and the variations in pore content across different size ranges. When analyzed in conjunction with the planar distribution model of pores in cementitious materials, it became apparent that standard cement mortar featured a relatively low proportion of tiny pores (5–200 μm) and large pores (>1000 μm). In contrast, medium-sized pores (500–1000 μm) and small pores (200–500 μm) constituted a larger proportion. This distribution is characteristic of mortar materials and plays a crucial role in shaping their mechanical properties and durability.

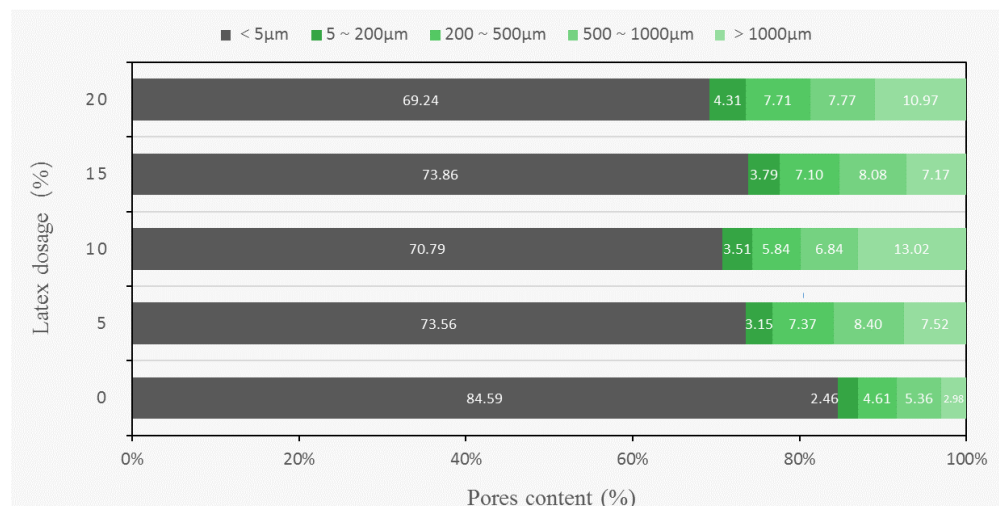


Figure 8. Evolution law of pore size in cement-based materials.

However, the incorporation of styrene butadiene latex generally increased the internal porosity of the cementitious materials. The growth in tiny pores (5–200 μm) was relatively moderate, while the increase in medium-sized (500–1000 μm) and small pores (200–500 μm) followed similar trends. It is worth noting that even with a 10% latex admixture in the modified mortar, the proportion of medium and small pores remained significant. Despite this, the most significant increase was observed in the content of large pores (>1000 μm), which had a detrimental impact on the overall performance of cementitious materials.

3.3. Influence Law of Porosity on Mechanical Properties of Cementitious Materials

The creation of porosity exerts a nuanced influence on the mechanical properties of cementitious materials. Specifically, excessive porosity and the presence of larger pores can have an adverse impact on the material's densification, resulting in a deterioration of its mechanical properties. However, the existence of smaller pores can yield beneficial effects on these properties, as demonstrated by various studies [33]. Testing was carried out following the guidelines specified in the Test Procedure for Cement and Cement Concrete in Highway Engineering (JTG 3420-2020) [29]. The experiments encompassed flexural and compressive strength tests conducted on cement mortar specimens, all of which were prepared using an identical proportionate mix. The testing process is depicted in Figure 9.

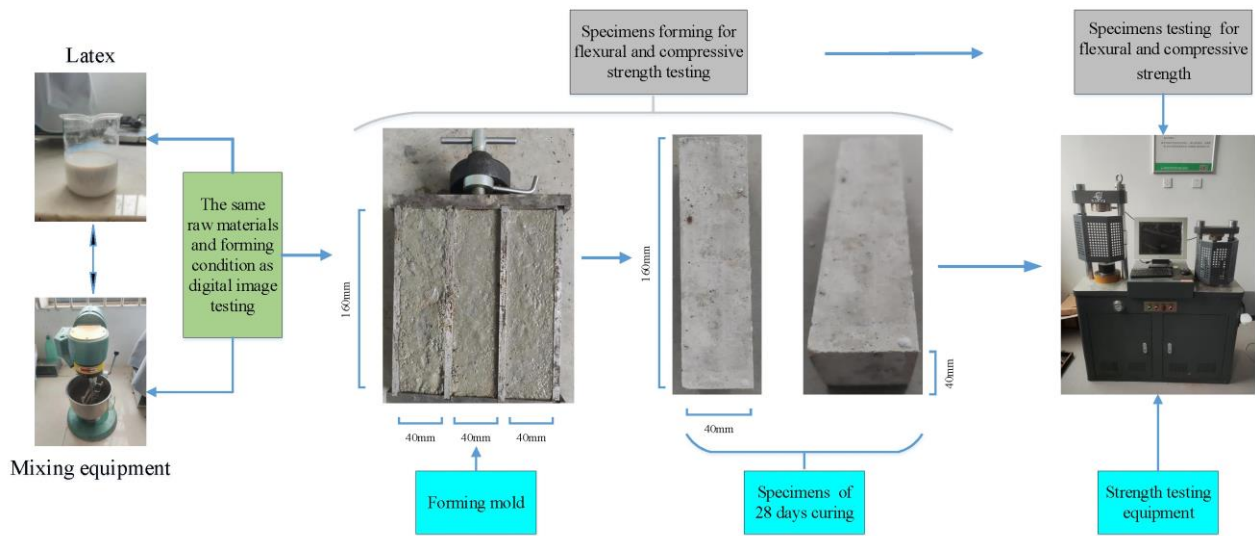


Figure 9. Flow chart of strength test for cementitious materials.

Figure 10 presents the correlation between the total number of pores and the flexural and compressive strength of cementitious materials. Generally, an inverse relationship exists: the greater the total number of pores, the more detrimental it is to the flexural and compressive strength of cementitious materials. However, a slight increase in pore count, corresponding to 5% and 15% latex doping, enhanced flexural strength. When the increase in total pores became too significant, there was a noticeable deterioration in flexural strength.

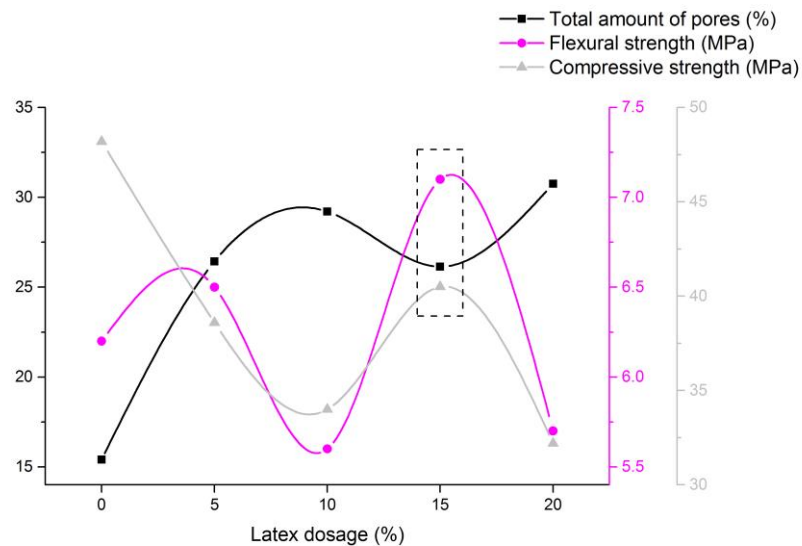


Figure 10. Effect of total porosity on the flexural and compressive strength of the cementitious materials.

The impact of pore count on compressive strength consistently indicated a weakening effect, suggesting that latex inclusion hinders the development of strength in cementitious materials. Interestingly, at 15% latex doping, a reduction in the total pore count aligns with an improvement of nearly 1 MPa in flexural strength and a lesser reduction in compressive strength. This implies that a reduction in pores could enhance the mechanical properties of the material. Conversely, at 10% latex doping, the presence of excessively large pores (>1000 μm) and a higher total pore count substantially impaired the mechanical properties of the material.

Figure 11 delves into the impact of various pore sizes on the flexural and compressive strength of the material. The data revealed a limited correlation between changes in flexural and compressive strength and the content of tiny pores (5–200 μm). Notably, at 15% latex doping, an increased concentration of these tiny pores corresponded to a favorable increase in flexural strength and a gradual reversal of the decreasing trend in compressive strength.

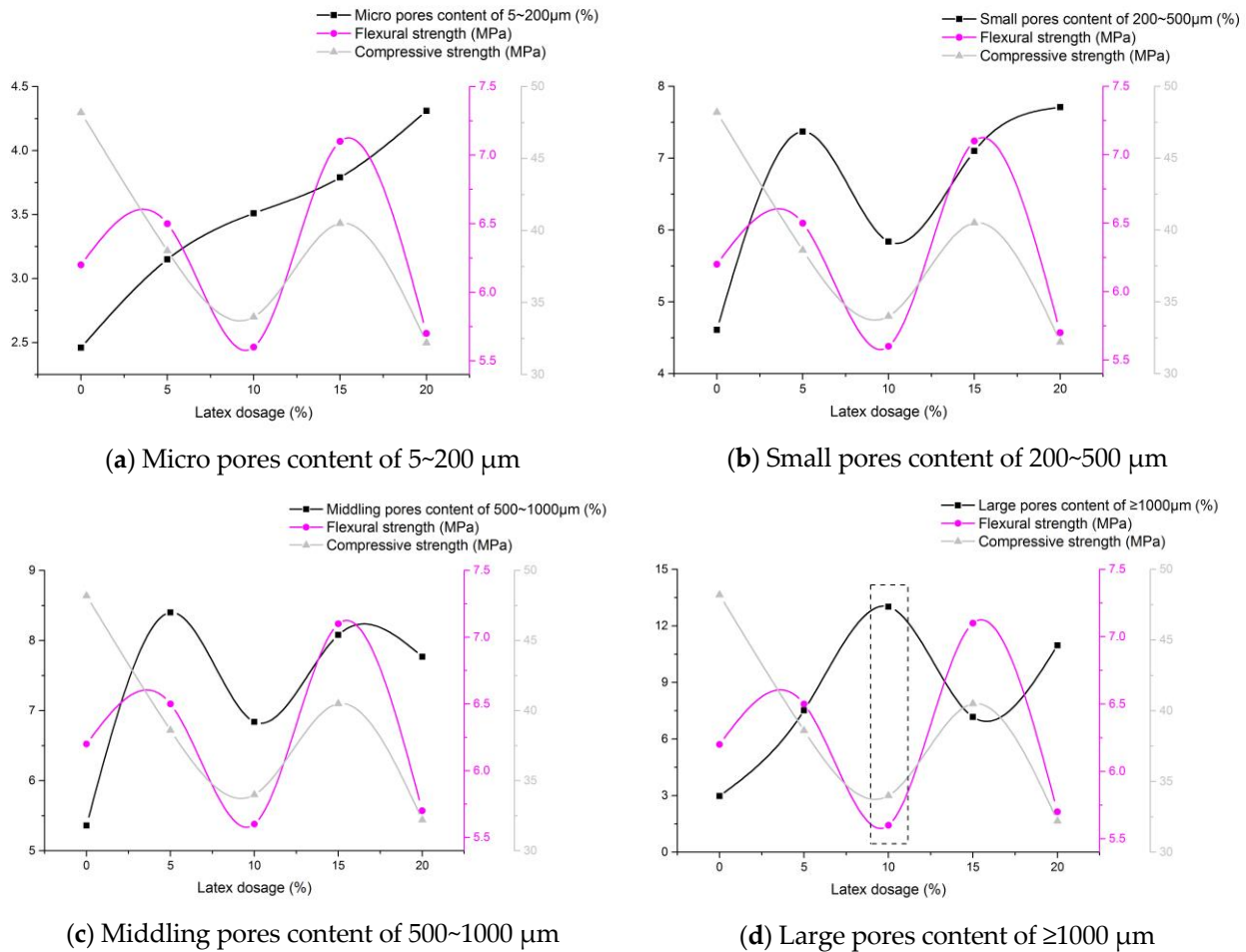


Figure 11. Effect of pore content with different size pores on the flexural and compression strength of the cementitious materials.

Figure 11b,c illustrates that the curves representing changes in the content of small pores (200–500 μm) and medium pores (500–1000 μm) roughly aligned with alterations in the flexural and compressive strengths of cementitious materials. This implies that an increase in the content of small and medium pores was beneficial for enhancing the mechanical properties of these materials. At 15% latex doping, both the decline in compressive strength and the improvement in flexural strength were moderated.

Figure 11d reveals that the curves reflecting changes in macropore content ($\geq 1000 \mu\text{m}$) were inversely related to the curves for both flexural and compressive strength in cementitious materials. This indicates that an increase in macropore content had a negative impact on the material's mechanical properties. Specifically, at 10% latex doping, the macropore content reached its peak, resulting in a significant decrease in both flexural and compressive strength. Conversely, at 15% latex doping, both the macropore content and total porosity were relatively low. This led to improved flexural strength and a less pronounced decrease in compressive strength, creating a more balanced relationship between these two mechanical properties. The effects on both flexural strength and compressive strength were relatively balanced.

In summary, the test results indicated that at low dosages, latex was unevenly dispersed throughout cementitious materials, resulting in relatively isolated pores that occupied limited space. During this phase, the viscoelastic properties of the latex improved the material's elasticity, enabling greater flexural deformation and mitigating stress concentration, thereby enhancing the material's flexural strength. However, as the latex dosage increased, it began to agglomerate within the cementitious matrix, introducing a significant number of air bubbles. While the viscoelastic nature of the latex initially contributed to filling and improving the matrix, the increased number of air bubbles began to compromise the material's structural integrity. This lack of compaction was exacerbated by the presence of a considerable number of large pores, severely undermining the mechanical properties of the material, particularly its compressive strength.

In essence, the mechanical properties of cementitious materials were influenced by both the total pore volume and the size distribution of these pores. When using admixtures, it was crucial to consider not only the overall pore count but also the specific distribution of pore sizes, especially the concentration of large pores ($>1000\ \mu\text{m}$). This comprehensive approach aided in the accurate evaluation of the material's mechanical properties and helped establish effective feedback mechanisms for optimizing admixture applications. Pore content analysis provided a microscopic lens through which to explore changes in the material's properties, and our tests validated the feasibility and precision of this method for assessing external influences. Unlike methods requiring expensive instrumentation, complex sample preparation, or intricate operational steps, our experimental study presented a cost-effective and straightforward approach for analyzing pore evolution in cementitious materials. This offered both a practical methodology and a theoretical foundation for enhancing the material's performance, optimizing admixture types, and determining appropriate dosages.

4. Conclusions

- (1) A characterization method was introduced for analyzing the pore distribution within this two-dimensional context, which involved enhancing image grayscale processing and binarization to achieve greater precision in distinguishing between pore-dense and pore-sparse regions. The distribution characteristics of pores of varying sizes in the two-dimensional structure of the materials were examined, and a pore distribution model was developed. Based on this model, the overall pore volume in the material, the distribution of pores across different size ranges, and the resulting impact on the material's mechanical properties were investigated. The key conclusions from this study included the following:
- (2) Analysis of the total pore volume within the complex solid–liquid–gas system of cementitious materials revealed that the addition of latex increased the overall porosity. Remarkably, when the latex dosage reached 15%, there was an inflection point in the increase in the total pore volume, after which it showed a modest rebound.
- (3) The pore content in all four categories tended to increase with the addition of latex. However, it was crucial to note that increasing the latex dosage did not linearly result in more significant porosity. This suggested that pore formation was influenced not just by the admixture itself but also by the interaction between the latex and the cementitious material, among other factors.
- (4) The study revealed that tiny pores marginally increased with higher latex dosages. In contrast to other pore sizes, the absolute content of tiny pores remained low, suggesting that latex additives had a limited impact. Small and medium pores behaved similarly with latex addition; both types showed a general increase but experienced a decline at a latex dosage of 10%.
- (5) In the case of large pores, the highest content was observed at 10% latex dosage, reaffirming the trend of smaller pores evolving into larger ones. These findings confirmed that smaller pores tended to develop into larger pores over time.

- (6) Higher porosity and micropore content generally weakened mechanical performance. However, at a small latex dosage, there was an improvement in flexural strength. When the latex dosage reached 15%, the total pore and micropore content declined, resulting in a balanced increase in flexural strength and a mitigated decline in compressive strength.
- (7) In the binarization process of planar images of cementitious materials using digital imaging techniques, a combination of automated threshold determination and manual comparison was employed to maximize accuracy. Despite these efforts, the method still has room for improvement, as it is susceptible to human error. Further research is necessary to enhance the quantitative accuracy of binarization thresholds.

Author Contributions: Methodology, Y.Y. and S.Z.; software, Z.H. and G.Y.; formal analysis, K.N.; investigation, B.T.; data curation, W.B. and Y.Y.; writing—original draft, Y.Y.; writing—review and editing, S.Z. and G.Y.; visualization, Z.H. and G.Y.; supervision, K.N., B.T. and L.C.; project administration, Y.Y. and S.Z. All authors have read and agreed to the published version of the manuscript.

Funding: This research was funded by 2021 Key Technology Projects of the Transportation Industry (grant number 2021-MS1-036), the Transportation Technology Project of Hainan province (grant number hizw20200903007; Qiong Jiao Ke Xin [2020] No. 293), the Technology Innovation and Demonstration Project of Yunnan Provincial Department of Transportation (2022-81), and the Yunnan Transportation Investment and Construction Group Co., Ltd. Technology Innovation Project (YCIC-YF-2021-09), and Science and Technology Plan Project of Yunnan Provincial Department of Science and Technology (202103AA080013). The funder had the following involvement with the study: the study design, collection, analysis, interpretation of data, the writing of this article, and the decision to submit it for publication.

Institutional Review Board Statement: Not applicable.

Informed Consent Statement: Not applicable.

Data Availability Statement: Data are contained within the article.

Conflicts of Interest: Author Y.Y. was employed by the company Chongqing Jiaotong University and Guangxi Nanbai Expressway Co., Ltd. The remaining authors declare that the research was conducted in the absence of any commercial or financial relationships that could be construed as a potential conflict of interest.

References

1. Han, J. *Research on the Performance of High-Performance Cement Concrete Pavement in Seasonal Frozen Areas*; Chang'an University: Xi'an, China, 2009; pp. 124–125. (In Chinese)
2. Czarnecki, L. Concrete-polymer composites: Trends shaping the future. *Int. J. Soc. Mater. Eng. Resour.* **2007**, *15*, 1–5. [[CrossRef](#)]
3. Ollitrault-Fichet, R.; Gauthier, C.; Clamen, G.; Boch, P. Microstructural aspects in a polymer-modified cement. *Cem. Concr. Res.* **1998**, *28*, 1687–1693. [[CrossRef](#)]
4. Li, Z.; Liang, N.; Wu, D.; Jing, W. Mechanism analysis of polymer cement-based materials. *J. Highw. Trans. Res. Dev.* **2005**, *2*, 63–66+86. (In Chinese)
5. Zhang, G.; Wang, P. Effect of hydroxyethyl methylcellulose on the formation of cement hydration products. *J. Build. Mat.* **2010**, *13*, 573–577. (In Chinese)
6. Yang, Z. *Research on the Control and Durability of Concrete Pore Structure in High Altitude Low Pressure Environment*; Chang'an University: Xi'an, China, 2023. (In Chinese)
7. Sakai, E.; Kasuga, T.; Sugiyama, T.; Asaga, K.; Daimon, M. Influence of superplasticizers on the hydration of cement and the pore structure of hardened cement. *Cem. Concr. Res.* **2006**, *36*, 2049–2053. [[CrossRef](#)]
8. Kondraivendhan, B.; Bhattacharjee, B. Effect of age and water-cement ratio on size and dispersion of pores in ordinary portland cement paste. *J. ACI Mat.* **2010**, *107*, 147–154.
9. Zhang, L.; Wang, W. Research on the influence of polymer on the pore structure and performance of foam concrete. *J. Concr. Cem. Prod.* **2011**, *185*, 9–12. (In Chinese) [[CrossRef](#)]
10. Wu, Z. Reflection on concrete science and technology. *J. Concr. Cem. Prod.* **1988**, *6*, 4–5. (In Chinese)
11. Wu, Z.; Lian, H. *High Performance Cement Concrete*; China Railway Press: Beijing, China, 1999. (In Chinese)
12. Wang, T.; Dra, Y.A.S.S.; Cai, X.; Cheng, Z.; Zhang, D.; Lin, Y.; Yu, H. Advanced cold patching materials (CPMs) for asphalt pavement pothole rehabilitation: State of the art. *J. Clean. Prod.* **2022**, *366*, 133001. [[CrossRef](#)]
13. Shen, A. *Cement and Cement Concrete*; Beijing Communications Press: Beijing, China, 2000; pp. 93–103. (In Chinese)

14. CEB European Committee on Concrete. *CEB Design Guidelines for Durable Concrete Structures*, 2nd ed.; Zhou, Y.; Di, X.; Han, J.; Cai, L., Translators; China Academy of Building Sciences: Beijing, China, 1989.
15. He, J. *Research on the Microstructure and Properties of Road Cement Concrete*; Chang'an University: Xi'an, China, 2009. (In Chinese)
16. Wang, T.; Li, M.; Cai, X.; Cheng, Z.; Zhang, D.; Sun, G. Multi-objective design optimization of composite polymerized asphalt emulsions for cold patching of pavement potholes. *Mater. Today Commun.* **2023**, *35*, 105751. [[CrossRef](#)]
17. Wang, T.; Weng, Y.; Cai, X.; Li, J.; Xiao, F.; Sun, G.; Zhang, F. Statistical modeling of low-temperature properties and FTIR spectra of crumb rubber modified asphalts considering SARA fractions. *J. Clean. Prod.* **2022**, *374*, 134016. [[CrossRef](#)]
18. Yan, X. *Study on the Influence of Pore Structure on the Salt Freezing Resistance of Cement-Based Materials*; Southeast University: Nanjing, China, 2015. (In Chinese)
19. Yang, W. *Effect of Inorganic Salts on Pore Structure and Frost Resistance of Concrete*; Harbin Institute of Technology: Harbin, China, 2009. (In Chinese)
20. Jo, B.W.; Park, S.K.; Kim, D.K. Mechanical properties of nano-MMT reinforced polymer composite and polymer concrete. *Constr. Build. Mater.* **2008**, *22*, 14–20. [[CrossRef](#)]
21. Pascal, S.; Alliche, A.; Pilvin, P. Mechanical behavior of polymer modified mortars. *J. Mater. Sci. Eng. A* **2004**, *380*, 1–8. [[CrossRef](#)]
22. Beeldens, A.; Gemert, D.V.; Ohama, Y. Integrated model of structure formation in polymer modified concrete. In Proceedings of the 11th International Congress on the Chemistry of Cement 2003, Durban, South Africa, 11–16 May 2003; pp. 206–216.
23. *JTG 3420-2020*; Test Regulations for Cement and Cement Concrete for Highway Engineering. People's Communications Press: Beijing, China, 2020.
24. Beeldens, A. Evolution in modeling microstructure formation in polymer-cement concrete: Restoration of buildings and monuments. *J. Restor. Build Monum.* **2013**, *19*, 97–108.
25. Abdulateef, Y.M.; Fahad, B.M.; Eweed, K.M. Repairing of concrete by using polymer-mortar composites. *Int. J. Mod. Eng. Res.* **2014**, *1*, 63–72.
26. Ukrainczyk, N.; Rogina, A. Styrene–butadiene latex modified calcium aluminate cement mortar. *Cem. Concr. Compos.* **2013**, *41*, 16–23. [[CrossRef](#)]
27. Petit, J.Y.; Wirquin, E. Evaluation of various cellulose ethers performance in ceramic tile adhesive mortars. *Int. J. Adhes. Adhes.* **2013**, *40*, 202–209. [[CrossRef](#)]
28. Bühler, T.; Zurbriggen, R.; Pieves, U.; Huwiler, L.; Raso, R. Dynamics of early skin formation of tiling mortars investigated by microscopy and diffuse reflectance infrared Fourier transformed spectroscopy. *Cem. Concr. Compos.* **2013**, *37*, 161–170. [[CrossRef](#)]
29. Ohama, Y. Principle of latex modification and some typical properties of latex-modified mortars and concretes. *J. ACI Mat.* **1987**, *84*, 511–518.
30. Pourchez, J.; Ruot, B.; Debayle, J.; Pourchez, E.; Grosseau, P. Some aspects of cellulose ethers influence on water transport and porous structure of cement-based materials. *Cem. Concr. Compos.* **2010**, *40*, 242–252. [[CrossRef](#)]
31. Bülchen, D.; Kainz, J.; Plank, J. Working mechanism of methyl hydroxyethyl cellulose (MHEC) as water retention agent. *Cem. Concr. Compos.* **2012**, *42*, 953–959. [[CrossRef](#)]
32. Ahmed, S.F.U. Mechanical and durability properties of mortars modified with combined polymer and supplementary cementitious materials. *J. Mater. Civil. Eng.* **2011**, *23*, 1311–1319. [[CrossRef](#)]
33. Tabassi, A.A.; Ramli, M. Effects of different curing regimes on engineering properties of polymer-modified mortar: An experimental study. *J. Mater. Civil. Eng.* **2012**, *24*, 468–478.
34. Linares-Unamunzaga, A.; Pérez-Acebo, H.; Rojo, M.; Gonzalo-Orden, H. Flexural strength prediction models for soil–cement from unconfined compressive strength at seven days. *J. Mater.* **2019**, *12*, 387. [[CrossRef](#)]
35. Tran, V.Q. Hybrid gradient boosting with meta-heuristic algorithms prediction of unconfirmed compressive strength of stabilized soil based on initial soil properties, mix design and effective compaction. *J. Clean. Prod.* **2022**, *355*, 131683. [[CrossRef](#)]

Disclaimer/Publisher's Note: The statements, opinions and data contained in all publications are solely those of the individual author(s) and contributor(s) and not of MDPI and/or the editor(s). MDPI and/or the editor(s) disclaim responsibility for any injury to people or property resulting from any ideas, methods, instructions or products referred to in the content.